Substrate Guided-Wave-Based Optical Interconnects for Multiwavelength Routing and Distribution Networks

Jian Liu, *Member, IEEE, Member, OSA,* and Ray T. Chen, *Member, IEEE*

***Abstract*— A two-dimensional (2-D) wavelength division demultiplexing (WDDM) device is demonstrated to separate and to distribute multiwavelength optical signals by employing substrate-guided wave optical interconnects. Working principle and power budget issues are analyzed. In this planarized architecture, stacked/multiplexed input holographic gratings and arrays of output holographic gratings are designed to be fabricated on the same waveguiding plate to steer multiwavelength optical signals into different routing directions, to zigzag within a waveguiding substrate, and then to be surface-normally coupled out of the substrate. A dual-wavelength routing and distribution network is demonstrated in experiment at 780 nm and 790 nm. The crosstalk is measured to be > -30 dB. The fan-out energy fluctuation is within $\pm 10\%$ for each wavelength. We also demonstrate a planar three wavelength optical network to separate and distribute three wavelengths at 760, 790, and 820 nm. It is feasible for this structure to be used as high capacity wavelength division demultiplexing and routing networks at center wavelengths of 800, 1330, and 1550 nm.**

***Index Terms*— Optoelectronic interconnects, optical networks, photopolymer films, volume hologram, wavelength division multiplexing (WDM).**

I. Introduction

OPTICAL interconnection has been widely agreed to be one of the most important alternatives to overcome the bottlenecks of electrical interconnects caused by electromagnetic interference, parasitic capacitance, and inductance coupling [1], [2]. For practical optical interconnections, precise alignment of the device components is required along with mechanical robustness and temperature stability. Free-space optical interconnects using conventional optomechanical technology are vulnerable to mechanical and environmental perturbations. Consequently, various planarized implementations were proposed to fold three-dimensional (3-D) optical systems into a two-dimensional (2-D) geometry and integrate them onto a single substrate with the light signals traveling inside the substrate [3]–[8]. By integrating photopolymer holographic optical elements (HOE's) with the designed diffraction efficiencies on planar waveguiding plates, substrate-guided wave optical interconnects were proposed and energy-equalized fan-out distribution has been solved [4]–[6]. Optical correlator and Fourier transformation were demonstrated by Reinhorn and his colleague using substrate-guided wave optical interconnects [7], [8]. In this paper, a two-dimensional (2-D) wavelength division demultiplexer (WDDM) serving both functions of wavelength separation and of 1-to-many fan-out signal distribution is proposed and demonstrated experimentally using the substrate guided-wave configuration.

With the development of passive optical networks, cost effectiveness and system compatibility are becoming critical issues to be solved. When passive optical networks are applied to local area networks (LAN's) like fiber-to-the-curb (FTTC), fiber-to-the-home networks (FTTH) [9], and multisensor systems [10], it becomes a necessity to route separate wavelength channels and to distribute each channel to many users. Fig. 1 shows an example of a fiber distribution network. When optical signals are transmitted to optical network units (ONU), and then distributed to subscribers, passive $1 \times N$ routers (PR) and passive $1 \times N$ splitters (PS) are desired to fulfill both wavelength routing and channel distribution. In our design shown in Fig. 2, stacked/multiplexed transmission volume holograms are employed as the input couplers to steer input optical signals with different wavelengths to their desired directions within a waveguiding plate, and then coupled out of the substrate by the output holographic optical element (HOE) arrays. Such a two-dimensional network configuration, having both the input and output HOE's integrated on one waveguiding plate, simultaneously fulfills wavelength separation, routing, and distribution. This planar architecture combines both the functions of the passive $1 \times N$ routers and the passive $1 \times N$ splitters shown in Fig. 1. It is obvious that this two-dimensional network configuration provides a robust, reliable, surface-mountable, and cost-efficient device with combined functions of wavelength demultiplexing and distributing.

To delineate the basic physics making the device plausible, working principle of transmission volume holograms targeted at the generation of substrate guided-wave optical interconnects is reviewed in Section II. Power budget consideration of the substrate-guided wave optical interconnects is given in Section III. Section IV describes design and fabrication of a multiwavelength 2-D wavelength division demultiplexer. Experimental results of a dual-wavelength and a triple-wavelength routing and distribution networks are presented in this section as well. Section V gives the concluding remarks.

Manuscript received August 31, 1998; revised November 3, 1998. This work was supported by the Ballistic Missile Defense Organization, Army SSDC, the DARPA, Office of Naval Research, Cray Research, DuPont, Lightpath, and the Advanced Technology Program (ATP) of Texas.

The authors are with Microelectronics Research Center, Department of Electrical and Computer Engineering, University of Texas at Austin, Austin, TX 78758 USA.

Publisher Item Identifier S 0733-8724(99)01208-6.

0733–8724/99$10.00 © 1999 IEEE

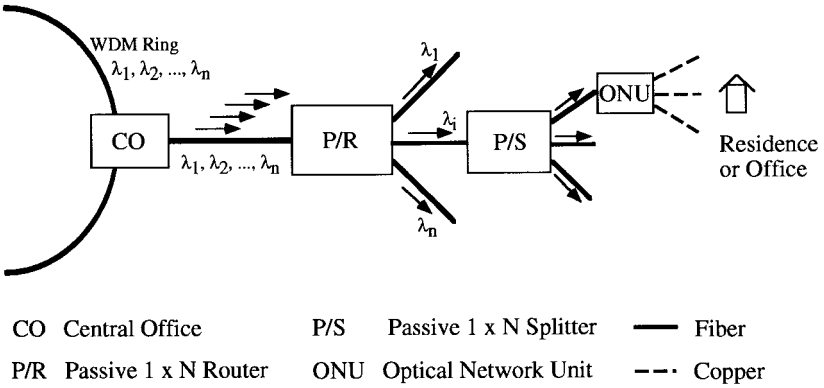

Fig. 1. An example of fiber distribution networks.

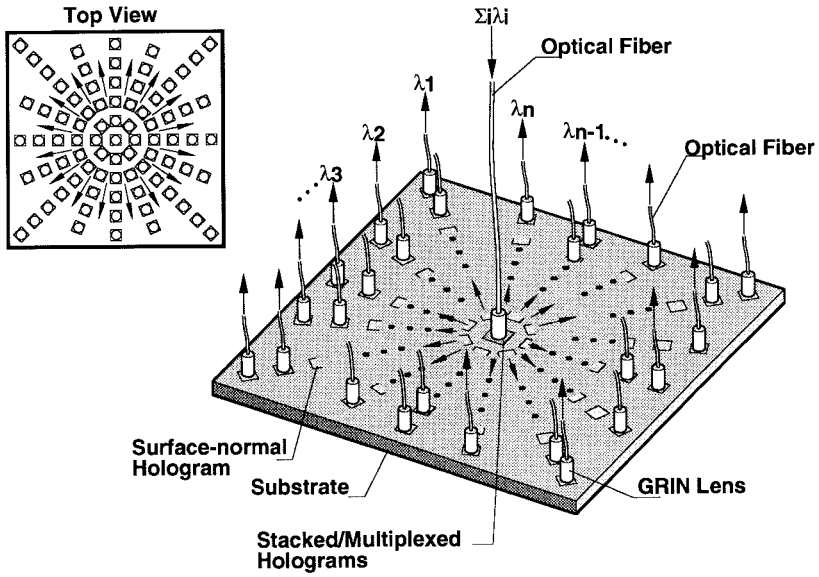

Fig. 2. Schematic diagram of a two-dimensional WDDM distributing network using substrate-guided wave optical interconnects.

II. Working Principle

For a transmission volume hologram with an input optical signal incident at an angle of θ with respect to the surface normal direction, if the polarization of the input optical signal is either parallel or perpendicular to the holographic grating vector, there should be no cross-coupling occurred. For an s-polarized optical signal, the diffraction efficiency is [11]

$$\eta_s = \sin^2(\gamma_s^2 + \xi^2)^{1/2}/(1 + \xi^2/\gamma_s^2) \tag{1}$$

where

$$\gamma_s = \frac{\kappa_s d}{(c_R c_S)^{1/2}}, \tag{2}$$

$$\xi = \Delta\theta \cdot K\, d\sin(\varphi - \theta)/2c_s - \Delta\lambda \cdot K^2\, d/8\pi n c_s \tag{3}$$

$$c_R = \cos\theta, c_s = \cos\theta - \frac{K}{\beta}\cos\varphi \tag{4}$$

and

$$\beta = \frac{2\pi n}{\lambda}, \quad K = \frac{2\pi}{\Lambda}, \quad \text{and} \quad \kappa_s = \frac{\pi\Delta n}{\lambda}. \tag{5}$$

The schematic representing such a diffraction is shown in Fig. 3(a). In (1)–(5), Δn is the amplitude of the refractive index modulation, θ is the angle of the incident optical signal within the hologram medium, Λ is the grating period, d is the thickness of the grating layer, λ is the free-space wavelength of incident light, n is the average refractive index of the grating medium, and φ is the slanted angle of the grating. Equation (3) gives a dephasing parameter in which $\Delta\theta$ is a small amount of angular deviation from the Bragg condition at an angle of incidence of θ, while $\Delta\lambda$ is the wavelength deviation from the Bragg condition for a fixed wavelength λ.

Fig. 3(b) shows a typical substrate guided-wave optical interconnect with the surface-normal configuration. The diffraction angle θ_{diff} of the volume hologram is designed to be larger than the total internal reflection (TIR) angle in a glass substrate while the optical signal is incident from the surface-normal direction with $\theta_{\text{in}} = 0°$. Fig. 4 shows the simulation results of diffraction efficiencies versus refractive index modulation of a randomly polarized wave [4], and the angular and wavelength deviation effects. The results are derived for films with a thickness of 20 and 100 μm, respectively, and with a refractive index $n = 1.52$ at $\lambda = 790$ nm and with a diffraction angle θ_{diff} of 45°. For the film thickness of 100 μm, the corresponding refractive index

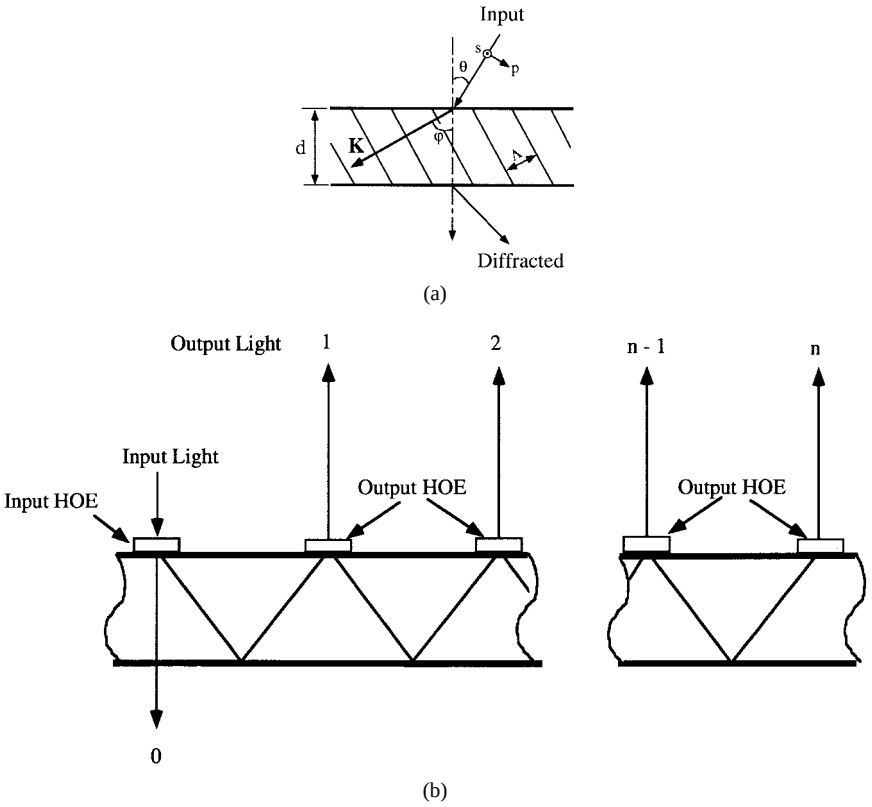

Fig. 3. (a) Schematic diagram of a transmission volume hologram and (b) a typical structure of substrate-guided wave optical interconnects.

modulation Δn used for simulating the effects of angular and wavelength changes is 0.0038 for a 93% diffraction efficiency at 790 nm. The parameters used for the 20-μm thick film are the same as those of the 100-μm thick film except that $\Delta n = 0.0184$ for the 20-μm thick film. Fig. 4(b) shows that the 3 dB bandwidth of the 100-μm thick film at a center wavelength of 790 nm with a diffraction angle θ_{diff} of 45° is 8 nm. And it is 40 nm for the 20-μm thick film. Fig. 4(c) shows the angular deviation tolerances. The 3 dB acceptance angles are 1.7 and 0.4° for the 20-μm thick film and the 100-μm thick film, respectively. From (3), we can see that the 3 dB wavelength bandwidth is inversely proportional to the film thickness for a fixed setting of the incident beam and the grating slanted angle.

When the input wavelength changes from λ to $\lambda + \Delta\lambda$ at a fixed incident angle, the diffraction angle changes from θ_{diff} to $\theta_{\text{diff}} + \Delta\theta_{\text{diff}}$. The dispersion relation is given by [12]

$$\Delta\theta_{\text{diff}}/\Delta\lambda = 2\tan\theta_{\text{diff}}/\lambda. \tag{6}$$

The lateral separation Δl of two optical signals with wavelengths of λ and $\lambda + \Delta\lambda$ is given by

$$\Delta l = 2md[\tan(\theta_{\text{diff}} + \Delta\theta_{\text{diff}}) - \tan\theta_{\text{diff}}] \tag{7}$$

where the integer m represents the number of the zig-zagged light paths within the waveguiding plate. It is shown that the channel crosstalks can be reduced at the output location for a designed wavelength as the lateral deviation occurs for other channel wavelengths.

III. Power Budget Consideration of Substrate Guided-Wave Optical Interconnects

Take I_0 as the intensity of input optical signal at wavelength of λ, I_i the intensity of output optical signal coupled out by the ith HOE [Fig. 2(b)] with diffraction efficiency of η_i, δ_1 the loss due to the Fresnel reflection and scattering at the interface between the air and the photopolymer film, and δ_2 the loss due to light scattering and attenuation at the interface of polymer film and the glass plate, and in the polymer film. The output intensity of optical signal emerging from the ith output coupler is then derived and given by [4], [13]

$$\begin{aligned} I_i &= \eta_0 I \prod_{k=1}^{i=1}(I-\eta_k)\eta_i \\ &= \eta_0 I_0 \prod_{k=1}^{i-1}(1-\eta_k)\eta_i(1-\delta_1)^2 \\ &\quad \cdot (1-\delta_2)^{i+1} e^{-(\alpha_i+\alpha_s)[2(i-1)d\tan\theta_{\text{diff}}+x_0]} \end{aligned} \tag{8}$$

where α_i and α_s are the absorption coefficient and the scattering coefficient of the glass, respectively, and x_0 the initial propagation distance of optical signal from the input coupler to the first output coupler (the minimum distance is $2d\tan\theta_{\text{diff}}$). $(1-\delta_1)^2$ and $(1-\delta_2)^{i+1}$ relate to the losses of the ith output optical signal passing through the film/air interfaces two times and passing through the films $i+1$ times, respectively. In general, besides the $\alpha_i + \alpha_s$, other parameters are all process-related. Deviation of the required diffraction efficiency of the HOE at the recorded position, cleanliness of the substrate, film-laminating process, and nonideal interface

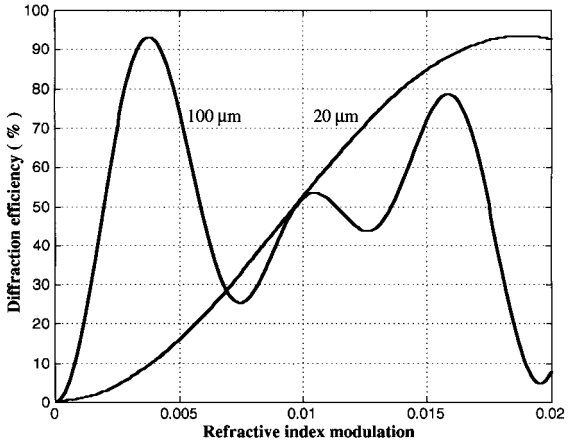

(a)

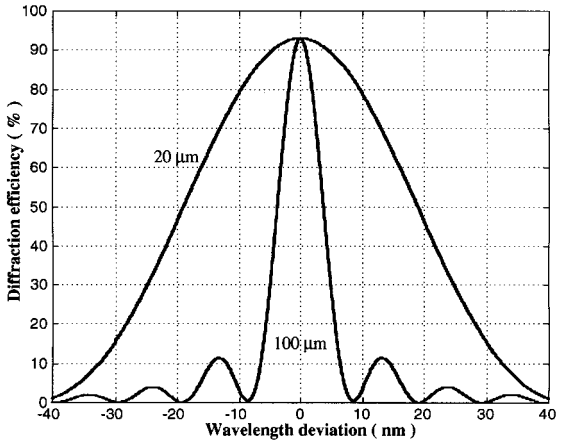

(b)

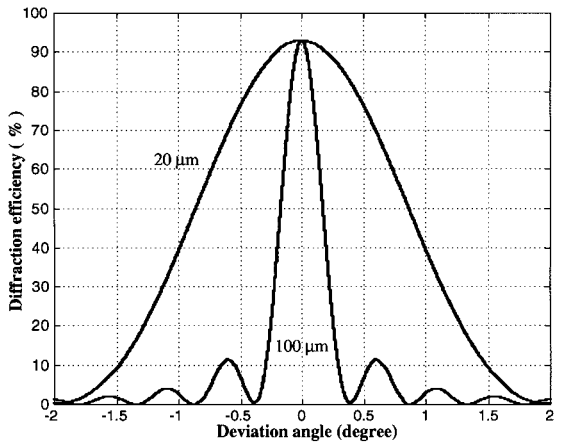

(c)

Fig. 4. Simulation results of diffraction efficiency as a function of (a) refractive index modulation, (b) wavelength deviation, and (c) angular deviation, for photopolymer films with thicknesses of 100 and 20 μm at 790 nm under a randomly polarized wave.

quality between the glass plate and the photopolymer film, all have effects on the output intensity of the optical signal, and then cause nonuniform fan-out energy distribution as well.

In practice, the diffraction efficiency adjustment of each HOE is always required based on the highest achievable efficiency. The maximum efficiency is measured to be η_M. To equalize fan-out energy distribution $I_1 = I_2 = \cdots = I_i = \cdots = I_n$, the diffraction efficiencies of the corresponding output HOE's are given by

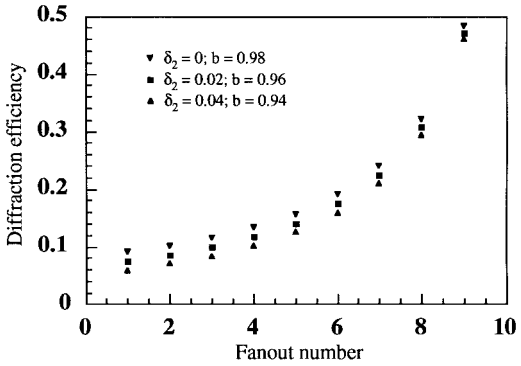

Fig. 5. Calculated diffraction efficiencies required for a 1-to-10 energy-equalized fan-out device. The last HOE, which is not shown in the figure, is with diffraction efficiency of 93% for the three cases.

$$\begin{aligned} \eta_n &= \eta_M \\ \eta_{n-1} &= \frac{\eta_n(1-\delta_2)e^{-2\alpha d\tan\theta_{\text{diff}}}}{1+\eta_n(1-\delta_2)e^{-2\alpha d\tan\theta_{\text{diff}}}} \\ &\cdots \\ \eta_{i-1} &= \frac{\eta_i(1-\delta_2)e^{-2\alpha d\tan\theta_{\text{diff}}}}{1+\eta_i(1-\delta_2)e^{-2\alpha d\tan\theta_{\text{diff}}}} \\ &\cdots . \end{aligned} \tag{9}$$

The overall efficiency of the 1-to-many fan-out device is defined as the total amount of optical power coupled out of the device divided by the total power of the input optical signal, that is

$$\eta_{\text{total}} = \frac{\sum_{i=1}^{n} I_i}{I_0}. \tag{10}$$

From (8) to (10), we can see that δ_2, α_i, and α_s affect the designed diffraction efficiencies of the output HOE's, while δ_1 affects only the total efficiency η_{total}. Fig. 5 shows the required diffraction efficiencies of a device with a 1-to-10 energy equalized fan-out distribution under three different cases. The parameters we used for the three cases is $\eta_M = 93\%, \delta_1 = 6\%$, and $x_0 = 2d \cdot \tan(\theta_{\text{diff}})$. In Fig. 5, b is used to represent the exponential item in (9), i.e., $b = \exp[-2(\alpha_i + \alpha_s)d\tan\theta_{\text{diff}}]$. The overall efficiencies of these three cases are calculated to be 75, 58, and 44%, respectively. If the absorption and scattering coefficients become larger, their effects on the energy uniformity and overall efficiency of the 1-to-many fan-out device can not be neglected, and have to be taken into consideration.

Among all the aforementioned factors, the accuracy of diffraction efficiency is the primary concern affecting the uniform fan-out energy distribution. This is similar to those described for surface-relief-grating-based array illuminators [13], [14]. Assume the diffraction efficiency of the ith HOE is η_i for an energy equalized 1-to-many fan-out under a specific polarization. If a deviation of $\pm\Delta\eta_i$ occurs for the ith output HOE, the diffraction efficiency becomes

$$\eta_i' = \eta_i \pm \Delta\eta_i. \tag{11}$$

The output intensity from the ith output HOE in (8) is then rewritten by

$$I_i' = \eta_0 I \prod_{j=1}^{i-1}(1-\eta_j')\eta_i' \tag{12}$$

where I is that defined in (8) and η_0 is the diffraction efficiency of the input HOE. The average light intensity I_{av} for such a 1-to-many fan-out device is given by

$$I_{\text{av}} = \frac{\eta_0}{n}\sum_{i=1}^{n}\prod_{j=1}^{i-1}(1-\eta_j')I\eta_i' \tag{13}$$

and the intensity fluctuation ε_i occurred at the ith output light signal can be written as

$$\varepsilon_i = \frac{I_i' - I_{\text{av}}}{I_{\text{av}}}. \tag{14}$$

IV. A 2-D WDDM Network

For the 2-D WDDM network in Fig. 2, we propose a planarized architecture having the input and the output volume holograms integrated on the same waveguiding substrate at their designated positions. This structure is robust to environmental and mechanical changes. By combining both functions of wavelength routing and distribution, many users may share the same source with this distributed 2-D WDDM. Either stacked or multiplexed volume holograms are able to be used as the optical wavelength routing filters to couple input optical signals $\lambda_1, \lambda_2, \cdots$, and λ_n into their designed routing directions as depicted in the architecture shown in Fig. 2. The bouncing angle within the waveguiding substrate is greater than the critical angle of the substrate. The separated optical signals propagate within the waveguiding substrate with total internal reflection and are distributed to their respective destinations, and then coupled out surface-normally by the arrays of cascaded volume holograms.

Fig. 6 shows the phase matching condition for the input volume holographic grating couplers of the 2-D WDDM network. Three phase-matching diagrams for the $(i-1)$th, ith, and $(i+1)$th input volume holograms separating respective wavelengths of λ_{i-1}, λ_i, and λ_{i+1}, respectively, are specified in this figure. The ith volume holographic grating has the input wave vector $\boldsymbol{ki}$ ($|\boldsymbol{k_i}| = 2\pi n/\lambda_i$) phase-matched with the grating vector $\boldsymbol{K_i}$ ($|\boldsymbol{K_i}| = 2\pi/\Lambda_i$), and so do $\boldsymbol{k_{i-1}}$ ($|\boldsymbol{k_{i-1}}| = 2\pi n/\lambda_{i-1}$) with $\boldsymbol{K_{i-1}}$ ($|\boldsymbol{K_{i-1}}| = 2\pi/\Lambda_{i-1}$) and $\boldsymbol{k_{i+1}}$ ($|\boldsymbol{k_{i+1}}| = 2\pi n/\lambda_{i+1}$) with $\boldsymbol{K_{i+1}}$ ($|\boldsymbol{K_{i+1}}| = 2\pi/\Lambda_{i+1}$). n is the average refractive index of the holographic medium, and Λ_i is the ith grating period. The angle between the two adjacent projected grating vectors in XY plane defined to be parallel to the interfaces of the planar grating region is $alpha$. The diffraction angle of the gratings is θ. Note that the discrepancy of the lengths of the wave vectors in Fig. 6 is caused by the wavelength difference of the input optical signals. In fabrication, it is critical to make each input volume hologram phase-matched with its designed optical wavelength, propagating direction, and diffraction angle. By properly allocating the input and output volume holograms

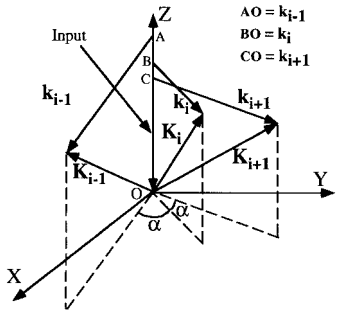

Fig. 6. Phase matching diagrams for stacked input volume holographic grating couplers.

at the desired wavelengths, it is able to realize multiple-wavelength channels separation and distribution. To get a small channel wavelength spacing, it is important to fabricate the input couplers with a narrow bandwidth. As discussed in Section II, the thicker the hologram, the narrower the channel wavelength spacing. In practice, it is not easy to get a thick emulsion for hologram recording (e.g., the commercially available DuPont photopolymer films have a maximum thickness of 100 μm). Fortunately, the dispersion properties of the volume holographic grating, as defined in (6) and (7), provide an alternative way to solve this problem [15].

It is promising for this 2-D configuration to be used for filtering and distributing different wavelength channels centered at 0.8, 1.3, and 1.55 μm. In a recent publication [16], a cascaded substrate-mode structure was proposed by Tsai *et al.*, to separate wideband wavelengths centered at 780, 1050, 1300, and 1550 nm using the wavelength selection properties of volume holographic gratings, and to separate interchannel wavelength spacing of 2 nm using the dispersion properties of the gratings. As the cascaded structure is stacked by waveguiding plates with holograms fabricated on the substrate surfaces, this device is not robust and not easy to be packaged for applications. By using our planarized architecture, we can stacked or multiplexed three bandpass volume holograms as input couplers to filter and route three separate wavelength groups centered at 0.8, 1.3, and 1.55 μm and to distribute them in three different directions to their designed output cascaded couplers. For each of the three grouped channels, dispersion properties can be used to separate interchannels with a much smaller wavelength spacing. All input and output holograms are integrated on the same waveguiding plate provides a robust, reliable structure. In the following, we focus on the experimental implementation of a dual-wavelength and of a triple-wavelength two-dimensional WDDM networks.

A. A Dual-Wavelength 2-D WDDM Network

In our experiment, Dupont photopolymer HRF 150 with 100 μm film thickness is chosen to fabricate the input holographic grating couplers. An Argon ion laser operating at 514 nm is used to record transmission volume holograms. A Ti: Sapphire tunable laser is employed to carry out the measurement. It is not able to obtain multiplexed hologram for DuPont photopolymer film HRF 150 with high-diffraction efficiencies due to the limited dynamic range of the refractive index

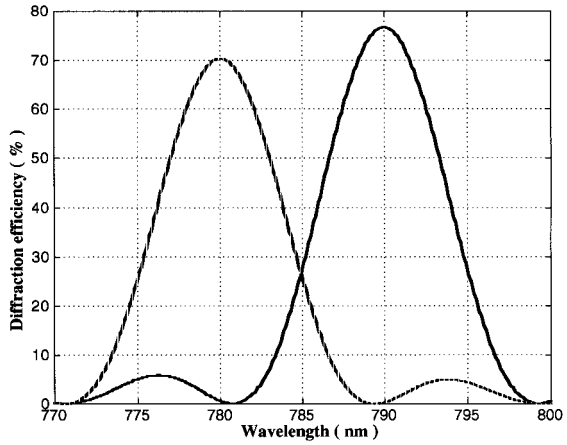

Fig. 7. Simulation results of diffraction efficiencies versus the wavelength deviation from central wavelengths 780 and 790 nm of a randomly polarized wave for 100-μm thick photopolymer films.

modulation. Consequently, two stacked holographic films are sequentially laminated and recorded on a quartz plate. The thickness of the substrate is 1.6 mm. The diffraction angle of the volume holographic gratings is 45°. The absorption and scattering coefficient α of the glass is measured to be $\sim$0.006 mm^{-1} at 790 nm (b of Fig. 5 is then calculated to be $\sim$0.98). The angle α between the two routing directions is designed to be 45°. One holographic grating is designed to deflect optical signal at $\lambda_1 = 790$ nm, and the other at $\lambda_2 = 780$ nm. Fig. 7 shows the simulation results of diffraction efficiencies versus the wavelength deviation from the central wavelengths 780 and 790 nm of randomly polarized waves with refractive index $n = 1.52$ for DuPont photopolymer films. The corresponding refractive index modulation Δn is 0.0027 for a 76% diffraction efficiency at 790 nm, and 0.0025 for a 70% diffraction efficiency at 780 nm. Two arrays of output holographic grating couplers are also sequentially fabricated along the desired routing direction for reconstruction wavelength at 780 and 790 nm, respectively, by employing DuPont photopolymer film HRF 600 with a 20-μm film thickness. The output coupler arrays with a relatively uniform fan-out distribution can be recorded by taking advantage of the fact that the collimated recording laser beam has a Gaussian intensity profile. Fig. 8 shows the experimental results taken by a CCD camera when the device operates at 780 and 790 nm. The diffraction efficiencies of the input holographic grating couplers are measured to be 70 and 76%, respectively. The 3 dB angular deviations of the volume holograms are measured to be within $\pm$0.25°. The two wavelengths are successfully separated and directed to their designed directions by the two stacked input holographic grating couplers. Each wavelength channel has ten fan-outs. The fan-out intensity distributions relative to the average light intensity for each wavelength are given in Fig. 8(b). The energy distribution nonuniformity is measured to be within $\pm$10%. The crosstalks between two channels are measured to be smaller than $-$30 dB. The channel crosstalks are reduced at the output location as the lateral deviation occurs for that channel with different wavelength as given in (7). The overall efficiencies for these two channels are measured to be 20% at 780 nm and 25% at 790 nm. Higher

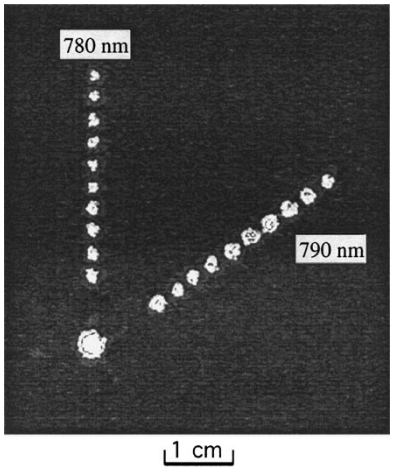

(a)

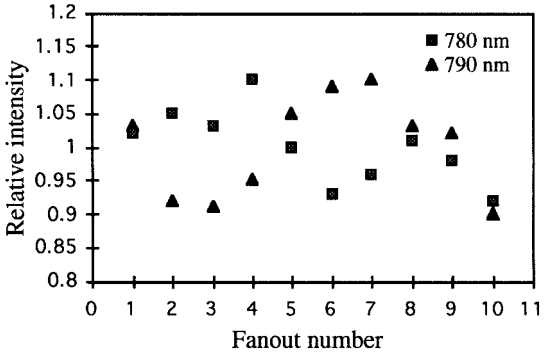

(b)

Fig. 8. Experimental results of the 2-D WDDM device while operating at 790 and 780 nm. (a) CCD image. Oblique fan-outs are for 790 nm channel. Vertical light spots corresponds to the 780 nm channel fan-outs. (b) Relative fan-out energy distributions.

overall efficiencies are not obtained due to the relatively lower diffraction efficiencies of the input holograms, and the shrinkage effects on the diffrcation efficiencies of the input and output volume holograms.

B. A Triple-Wavelength Routing and Distribution Network

Fabricating a triple-wavelength distribution network is also demonstrated. Three volume holograms are stacked on a glass substrate as input couplers to separate three optical channels. In our experiment, we found that it is difficult to stack three holograms by using the 100-μm thick photopolymer films. We, therefore, employ HRF 600 $\times$ 001–20 (20 μm thick) instead. Fig. 9 shows the simulation results for three volume holograms designed for separation of three optical channels with wavelengths centered at $\lambda_1 = 760$ nm, $\lambda_2 = 790$ nm, and $\lambda_3 = 820$ nm. The input optical signals are in the surface normal direction. The diffraction angle is designed to be at an angle of 48°. The angle between the two routing directions is designed to be 45°. Three arrays of output HOE's are recorded in DuPont photopolymer film HRF 600 with a 20-μm film thickness along the desired routing direction for reconstruction wavelengths at 760, 790, and 820 nm, respectively. These arrayed holograms are used to couple optical signals of the three wavelengths out of the glass substrate at the surface

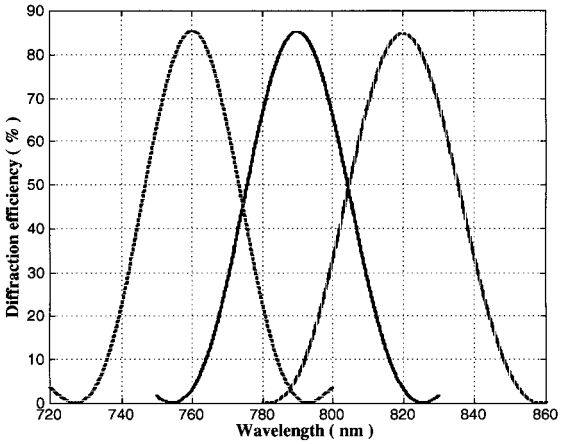

Fig. 9. Simulation results of diffraction efficiencies versus the wavelength deviation from central wavelengths 760, 790, and 820 nm of a randomly polarized wave for 20-μm thick photopolymer films.

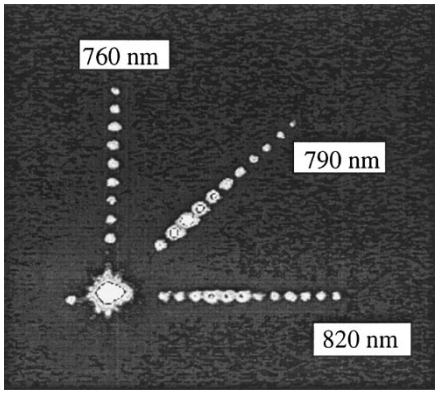

Fig. 10. Experimental results of the planar WDDM device while operating at 760, 790, and 820 nm.

normal direction. Fig. 10 shows the preliminary experimental results. We can see that the three wavelengths are successfully separated and steered to their designed directions by the three stacked input holographic grating couplers, and then coupled out by three separate HOE arrays. Nonuniform fan-out intensity distributions are observed, which are $\pm$15% for 760 nm, $\pm$55% for 790 nm, and $\pm$30% for 820 nm. The overall efficiencies are between 30 and 35%. Maximum crosstalk of -15 dB is observed in our experiment.

V. Discussion and Conclusions

Using substrate guided-wave-based optical interconnects, we demonstrate a cost-effective and user-sharing two-dimensional wavelength demultiplexing and distributing optical network with a planarized architecture. With the planar multiwavelength WDDM, optical signals at various wavelengths are separated and diffracted into the waveguiding plate in different routing directions by stacked/multiplexed holographic gratings, distributed within the waveguiding plate with total internal reflection, and coupled out of the substrate to each user by output holographic grating. This planarized architecture has advantages of large source-sharing capacity, robustness to environmental and mechanical perturbations, and relatively easy integration and fabrication. As the 3 dB wavelength bandwidth is inversely proportional to the film thickness, the channel wavelength spacing is limited to the photopolymer film thickness commercially available. Using dispersion properties of volume holograms, smaller channel wavelength spacing may be realized. In our experiments, we present a dual-wavelength routing and distributing network using the wavelength selection properties of the stacked volume holograms to separate two optical signals at wavelengths of 780 and 790 nm. The crosstalks are measured to be > -30 dB, and the nonuniformity of the fan-out energy distribution is within $\pm$10%. We also demonstrate a multiwavelength planar routing and distribution network which separates and distributes three wavelengths of 760, 790, and 820 nm with > -15 dB crosstalks.

Furthermore, it is feasible to realize multiwavelength channels routing and distribution centering at 0.8, 1.3, and 1.55 μm wavelengths by using this planarized architecture. The wavelength selectivity of the transmission volume holograms can be used to separate and route these three groups of channels into three different directions. The dispersion properties can then be used to further separate interchannels with a smaller wavelength spacing. Besides DuPont photopolymer films, dichromated gelatin (DCG) [17], [18] may be used as hologram recording material for the two-dimansional WDDM as well.

References

[1] J. W. Goodman, F. I. Leonberger, S. Y. Kung, and R. A. Athale, "Optical interconnection for VLSI systems," *Proc. IEEE*, vol. 72, pp. 850–866, 1984.
[2] T. Yatagai, S. Kawai, and H. Huang, "Optical computing and interconnects," *Proc. IEEE*, vol. 84, pp. 828–852, 1996.
[3] J. Jahns, "Planar packaging of free-space optical interconnections," *Proc. IEEE*, vol. 82, pp. 1623–1631, 1994.
[4] J. Liu, Z. Fu, and R. T. Chen, "Polarization sensitivity of photopolymer-based volume holograms for one-to-many surface normal optical interconnects," *Opt. Eng.*, vol. 37, pp. 660–665, 1998.
[5] J. Liu and R. T. Chen, "A two-dimensional dual-wavelength routing network with 1-to-10 cascated fanouts," *IEEE Photon. Technol. Lett.*, vol. 10, pp. 238–240, 1997.
[6] J. Liu, C. Zhao, R. Lee, and Ray T. Chen, "Cross-link optimized cascaded volume hologram array with energy-equalized one-to-many surface-normal fan-outs," *Opt. Lett.*, vol. 22, pp. 1024–1026, 1997.
[7] S. Reinhorn, Y. Amitai, and A. A. Friesem, "Compact planar optical correlator," *Opt. Lett.*, vol. 22, pp. 925–927, 1997.
[8] S. Reinhorn, S. Gorodeisky, A. A. Friesem, and Y. Amitai, "Fourier transformation with a planar holographic doublet," *Opt. Lett.*, vol. 20, pp. 495–497, 1995.
[9] I. P. Kaminow and T. L. Koch, *Optical Fiber Telecommunications IIIA*. New York: Academic, 1997.
[10] R. T. Chen, D. Robinson, H. Lu, M. R. Wang, T. Jannson, and R. Baumbick, "Reconfigurable optical interconnection network for multimode optical fiber sensor arrays," *Opt. Eng.*, vol. 31, pp. 1098–1105, 1992.
[11] H. Kogelnik, "Coupled wave theory for thick hologram gratings," *The Bell Syst. Tech. J.*, vol. 13, pp. 2909–2947, 1969.
[12] J. E. Ludman, "Approximate bandwidth and diffraction efficiency in thick holograms," *Amer. J. Phys.*, vol. 50, pp. 244–246, 1982.
[13] T. Nakaya, Y. Katoh, T. Kubota, and M. Tabeda, "Diffraction efficiency of a grating coupler for an array illuminator," *Appl. Opt.*, vol. 35, pp. 3891–3898, 1996.
[14] T. Kubota and M. Takeda, "Array illuminator using grating couplers," *Opt. Lett.*, vol. 14, pp. 651–652, 1989.
[15] M. M. Li and R. T. Chen, "Five-channel surface-normal wavelength-division demultiplexer using substrate-guided waves in conjunction with a polymer-based littrow hologram," *Opt. Lett.*, vol. 20, pp. 797–799, 1995.

[16] Y. K. Tsai, Y. T. Huang, and D. C. Su, "Multiband wavelength-division demultiplexing with a cascaded substrate-mode grating structure," *Appl. Opt.*, vol. 34, pp. 5582–5588, 1995.
[17] T. G. Georgekutty and H. K. Liu, "Simplified dichromated gelatin hologram recording process," *Appl. Opt.*, vol. 26, pp. 372–376, 1987.
[18] J. H. Yeh and R. K. Kostuk, "Substrate-mode holograms used in optical interconnects: Design issues," *Appl. Opt.*, vol. 34, pp. 3152–3164, 1995.

Jian Liu (M'97) received the B.S. and M.S. degrees in optics from Shandong University, Jinan, China, in 1986 and Shanghai Jiao Tong University, Shanghai, China, in 1989, respectively. He received another M.S. degree in electrical engineering from the University of New Orleans (UNO), LA, in 1996. He received the Ph.D. degree in electrical engineering from the University of Texas at Austin in 1999.

He was an Associate Professor at Qingdao University, Qingdao, China, where he was also a Coprinciple Investigator of several projects on Infrared Radiometry and High-Speed Holography sponsored by the National Natural Science Foundation of China. His research interests cover optoelectronic interconnects, optical networks, wavelength division demultiplexers, ellipsometry, polarization optics, diffractive optics, holography, and IR radiometry. He has authored or coauthored over 20 journal publications and over 15 conference presentations. He is the inventor of the corner-cube four-detector photopolarimeter, and a path-reversed wavelength division demultiplexer.

Dr. Liu is the recipient of the Distinguished Research Award of UNO in 1996, and two SPIE Educational Awards in 1997 and 1998. He is a member of SPIE, the Optical Society of America (OSA), AAAS, and Sigma Xi.

Ray T. Chen (M'91), photograph and biography not available at the time of publication.